

Article

Tailoring of Hydrotalcite-Derived Cu-Based Catalysts for CO₂ Hydrogenation to Methanol

Leone Frusteri ¹, Catia Cannilla ², Serena Todaro ³, Francesco Frusteri ² and Giuseppe Bonura ^{2,*}

¹ Dip Ing Elettronica, Chimica ed Ingegneria Industriale, Università di Messina, Contrada di Dio I, 98166 Messina, Italy; leone.frusteri@unime.it

² CNR-ITAE, Istituto di Tecnologie Avanzate per l'Energia "Nicola Giordano", Via S. Lucia sopra Contesse 5, 98126 Messina, Italy; catia.cannilla@itae.cnr.it (C.C.); francesco.frusteri@itae.cnr.it (F.F.)

³ Dip. Ing. Ambiente Territorio e Ing. Chimica, Università della Calabria, Via P. Bucci, 87036 Rende, Italy; serena.todaro@unical.it

* Correspondence: giuseppe.bonura@itae.cnr.it; Tel.: +39-090-624205; Fax: +39-090-624247

Received: 13 November 2019; Accepted: 9 December 2019; Published: 12 December 2019



Abstract: Ternary Cu_xZn_yAl_z catalysts were prepared using the hydrotalcite (HT) method. The influence of the atomic *x:y:z* ratio on the physico-chemical and catalytic properties under CO₂ hydrogenation conditions was probed. The characterization data of the investigated catalysts were obtained by XRF, XRD, BET, TPR, CO₂-TPD, N₂O chemisorption, SEM, and TEM techniques. In the "dried" catalyst, the typical structure of a hydrotalcite phase was observed. Although the calcination and subsequent reduction treatments determined a clear loss of the hydrotalcite structure, the pristine phase addressed the achievement of peculiar physico-chemical properties, also affecting the catalytic activity. Textural and surface effects induced by the zinc concentration conferred a very interesting catalyst performance, with a methanol space time yield (STY) higher than that of commercial systems operated under the same experimental conditions. The peculiar behavior of the hydrotalcite-like samples was related to a high dispersion of the active phase, with metallic copper sites homogeneously distributed among the oxide species, thereby ensuring a suitable activation of H₂ and CO₂ reactants for a superior methanol production.

Keywords: CO₂ hydrogenation; methanol synthesis; hydrotalcite; copper catalysts

1. Introduction

Methanol is usually produced from synthesis gas mixtures (CO_x/H₂) at typical reaction conditions of 230–280 °C and 50–100 bar over Cu-based catalysts. In this industrial process, a Cu-based catalyst is typically used, with the composition completed by Zn and Al components [1,2]. The development of ternary Cu/ZnO/Al₂O₃ catalysts for methanol synthesis was started in the 1960s and, since then, it was fine-tuned and optimized, without major changes in the formulation. There is a large consensus that copper represents the active phase for this reaction, and the primary role of ZnO is to create a definite metal-carrier interaction [3,4]. Incorporation of alumina into the catalyst formulation is instead essential for improving resistance to the thermal sintering of the Cu crystallites [5,6]. It is also demonstrated that alumina can act as a promoter, which specifically tailors the reduction properties of ZnO [7].

It is known that preparation of an industrial methanol catalyst involves the initial co-precipitation of a highly mixed CuZn(Al) hydroxycarbonate phase. This is usually realized by mixing of metal nitrate salts and sodium carbonate solutions under controlled pH and temperature. The subsequent aging step of the amorphous precipitate is fundamental for the formation of crystalline

hydroxycarbonate precursors [8–10]. On this account, studies on binary Cu_xZn_y preparations enabled a deep understanding of the more complex ternary (Cu/Zn/Al) systems. Therefore, in binary preparations, typical crystalline phases range from Cu-rich to Zn-rich compositions, including malachite $\text{Cu}_2(\text{OH})_2\text{CO}_3$, zincian malachite $(\text{Cu}_x\text{Zn}_y)_2(\text{OH})_2\text{CO}_3$, aurichalcite $(\text{Cu}_x\text{Zn}_y)_5(\text{OH})_6(\text{CO}_3)_2$, and hydrozincite $\text{Zn}_5(\text{OH})_6(\text{CO}_3)_2$. In particular, zincian malachite is currently considered to be the optimum precursor for the methanol synthesis catalyst, which facilitates formation of a highly porous meso-structure [11]. Considering that the maximum amount of Zn which can be substituted into the malachite lattice is 27 at.%, the optimum Cu:Zn molar ratio is close to 2:1 [12]. Higher Zn contents are desirable to facilitate further dilution of the Cu component, thereby enhancing metal dispersion, although this can result in a lower crystallinity of the zincian malachite phase. The final thermal decomposition of the hydroxycarbonates leads the formation of an intimate mixture of oxides, while an in situ reduction step is required to obtain the active catalyst.

Recent approaches to synthesize methanol via catalytic hydrogenation of CO_2 , as the key for an anthropogenic chemical carbon cycle along with the need to reduce the economic impact of the conventional high-pressure synthesis of methanol via syngas, now address the research efforts toward novel preparation methods suitable for obtaining catalytic systems characterized by high copper dispersion and surface basicity to enhance CO_2 adsorption [13–15], as the competitive reaction pathway of reverse water gas shift (RWGS) leads to a loss of methanol production [16,17]. Therefore, appropriate adsorption amount and adsorption strength of CO_2 are beneficial for the production of methanol, which give a guideline for the design of highly effective and efficient catalysts. On this account, considerable attention was recently paid to hydrotalcite-like compounds (HT) as catalyst precursors, because the catalyst systems derived from hydrotalcite structures possess homogeneous dispersion of metal cations at an atomic level, high stability against sintering, high specific surface area, and strongly basic properties [18–20].

In the present work, we inspected the catalytic behavior of CuZnAl catalysts as obtained from hydrotalcite-like structures in a CO_2 -to-MeOH hydrogenation reaction. Irrespective of the extent of crystallinity of the coprecipitated phase, the influence of the Cu:Zn:Al ratio on the formation of well-dispersed and active metal particles, generated after calcination and reduction, was addressed.

2. Results and Discussion

2.1. Physico-Chemical Properties

The list of the investigated catalysts with their main physico-chemical properties is presented in Table 1.

Table 1. List of catalysts, analytical composition, and textural properties.

Catalyst Sample	Analytical Comp. (wt.%) ^(a)			Zn/(Cu + Zn + Al)	S_{ABET} ^(b)	PV ^(b)	APD ^(c)
	CuO	ZnO	Al ₂ O ₃	(at/at)	(m ² /g)	(cm ³ /g)	(Å)
HT-111	37.5	38.4	24.1	0.33	74.7 ± 0.2	0.586	314
HT-122	23.1	47.3	29.6	0.40	62.3 ± 0.3	0.503	323
HT-121	27.1	55.5	17.4	0.50	28.6 ± 0.3	0.275	383
HT-112	30.2	31.0	38.8	0.25	136.0 ± 0.6	0.350	103
CuZnAl *	35.0	34.3	30.7	0.29	105 ± 1.1	0.231	88

* Commercial benchmark catalyst; (a) from XRF analysis by considering an oxide composition; (b) From N_2 ads/des isotherms at -196°C after H_2 reduction at 300°C and further passivation; (c) average pore diameter (APD, $4PV/S_{\text{ABET}}$).

Textural data show that the hydrotalcite synthesis route leads to systems characterized by different surface exposure, with values of total surface area decreasing with the ZnO content. In fact, the lowest S_{ABET} value (28.6 m²/g) was recorded at high (0.5) Zn/(Cu + Zn + Al) ratios, while the highest values (62.3–136.0 m²/g) were found for Zn/(Cu + Zn + Al) ratios ≤ 0.4 .

Within the range of composition considered, all hydrotalcite-like samples exhibit large values of cumulative pore volume (0.275–0.586 cm³/g), accounting for a trend of average pore diameter (APD) specular to that of surface area, thus being strongly dependent on the ZnO atomic fraction and increasing with it (Figure 1).

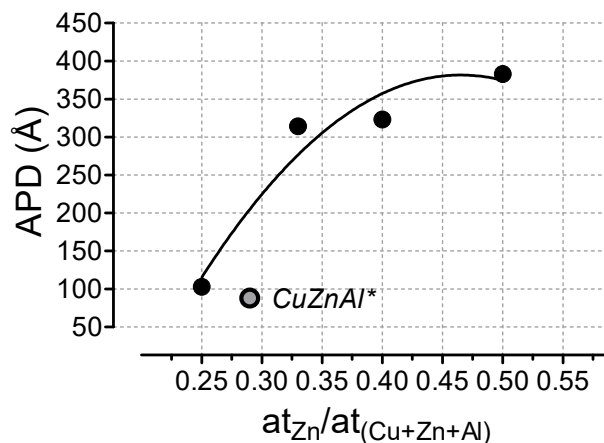


Figure 1. Effect of the Zn/(Cu + Zn + Al) atomic ratio on the average pore diameter (APD) of the hydrotalcite-like catalysts. * Reference CuZnAl catalyst.

To determine the typical structure formed during the preparation and its modification upon the treatments of calcination and reduction, an XRD analysis was preliminarily carried out. As it is possible to observe in Figure 2A, the representative “dried” catalyst sample (a) showed the characteristic reflections of the hydrotalcite phase, with clear evidence for the presence of (hydroxy)carbonate precursors, matching the pattern reported for the Cu₃Zn₃Al₂-(OH)₁₆CO₃·4H₂O phase (JCPDS 37–629). However, this phase was no longer retained after calcination, with a diffraction pattern (b) appearing without significant crystallinity, characterized by a prevalently amorphous architecture. Irrespective of the atomic ratio, no reflections of “isolated” CuO tenorite (JCPDS 41–0254) were detected in the calcined samples, while poorly crystallized mixed oxides phases of CuAl₂O₄ at 32.9° and 36.3° (JCPDS 33–0448) along with ZnAl₂O₄ at 32.1° and 36.8° (JCPDS 05–0669) were observed. Moreover, in the HT-122 sample, only few traces of low intensity in the 2θ range of 56°–70° revealed the presence of a hexagonal ZnO phase (JCPDS 36–1451). Upon reduction at 300 °C (see Figure 2B), the main peak at 43.4° was diagnostic of the formation of metallic copper (JCPDS 04–0836), with no evidence for residual presence of the spinel CuAl₂O₄ structure, while the ZnAl₂O₄ phase was still present. Yet, although Cu₂O was detected in none of the diffraction patterns, interestingly, in the HT-112 sample (d), a metastable mixed-valence oxide Cu₄O₃ (JCPDS 03–0879) could be also observed at 28.0° and 30.3°.

TPR measurements, carried out in order to shed light onto the effects of the preparation method and catalyst composition on the reduction kinetics of the investigated catalysts, are shown in Figure 3. All samples displayed a main H₂ consumption peak centered at 278–296 °C (see also Table 2), diagnostic of a quantitative reduction of CuO to metallic Cu below 350 °C, whereas the slight differences in both the onset reduction ($T_{o,red}$) and the maxima temperature (T_{max}) can be explained on the basis of the extent of copper-oxide(s) interaction, affected by the different metal loading in the hydrotalcite samples. A shoulder on the left side of the maximum was particularly evident at high Zn content, becoming wider and splitting in the HT-121 sample (profile c), signaling a different kinetic reduction dependent on the size of crystalline CuO particles, as a measure of heterogeneity of the copper distribution.

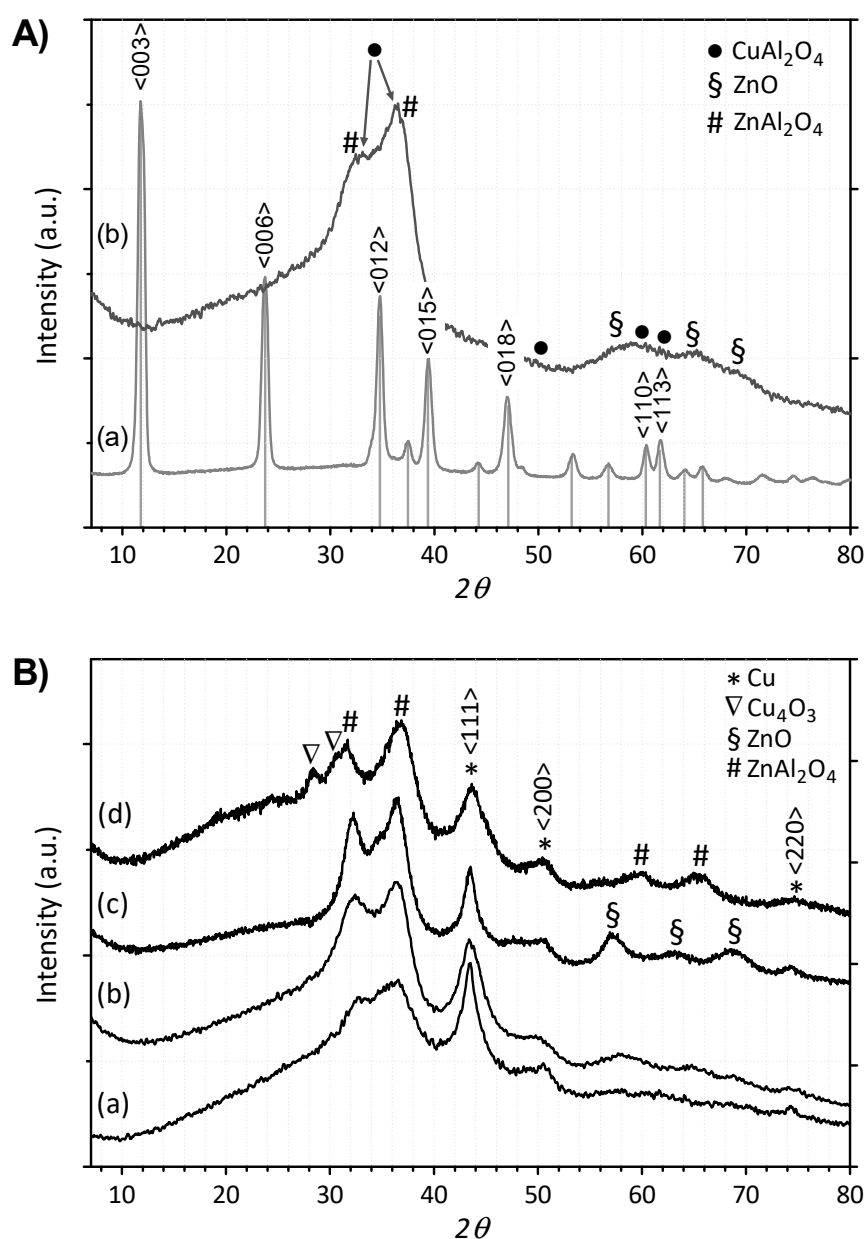


Figure 2. XRD patterns of the hydrotalcite-like $\text{Cu}_x\text{Zn}_y\text{Al}_z$ catalysts. (A) Structural modifications observed on the HT-122 sample: (a) as “dried”; (b) upon “calcination”. (B) Comparison of the “reduced” samples: (a) HT-111; (b) HT-122; (c) HT-121; (d) HT-112.

The amount of hydrogen consumption corresponded to the stoichiometric amount (0.97) for CuO reduction only for the HT-111 sample, while, for the HT-112 sample, an H_2/Cu ratio of 1.09 suggested a total reduction of copper oxide associated with a partial reduction of ZnO and/or Al_2O_3 in interaction with the copper crystallites, capable of storing large amounts of hydrogen both on the surface and in subsurface regions [21]. As a general behavior, within the range of composition investigated, the Zn atomic fraction was seen to linearly affect the extent of copper reduction (see Figure 4), such that a higher Zn content (like in HT-122 and HT-121) led to a greater reduction of CuO . Moreover, the baseline drift observed at $T > 350^\circ\text{C}$, with a poorly resolved temperature maximum, was associated with an ongoing reduction of the ZnO promoter [6].

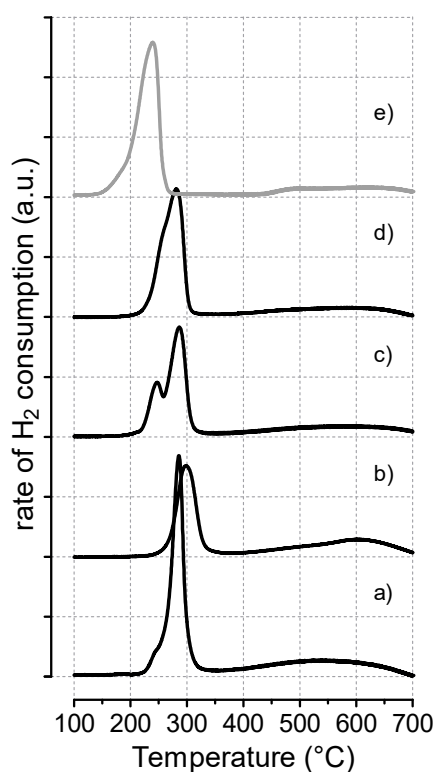


Figure 3. TPR profiles of the $\text{Cu}_x\text{Zn}_y\text{Al}_z$ catalysts and reference sample: (a) HT-111; (b) HT-122; (c) HT-121; (d) HT-112; (e) CuZnAl.

Table 2. TPR data. Extent of hydrogen consumption, onset temperature of reduction ($T_{o,\text{red}}$), and temperature of peak maxima (T_{Mi}).

Catalyst Sample	H_2 -TPR			
	mmol $\text{H}_2/\text{g}_{\text{cat}}$	$T_{o,\text{red}}$ ($^\circ\text{C}$)	T_{max} ($^\circ\text{C}$)	H_2/Cu ^(a)
HT-111	4.9	202	286	0.97
HT-122	3.9	170	278	0.86
HT-121	4.2	174	283	0.75
HT-112	4.3	206	296	1.09
<i>CuZnAl</i> *	5.2	137	237	0.94

* Commercial benchmark catalyst: (a) in the T range: 100–350 $^\circ\text{C}$.

The TPR profile of the reference catalyst (e) was similar to that of hydrotalcite-like catalysts, with a main peak centered at 237 $^\circ\text{C}$ and markedly skewed on the low-T side ($T_{o,\text{red}} = 137$ $^\circ\text{C}$), accounting for an almost stoichiometric H_2/Cu ratio (0.94). Above 350 $^\circ\text{C}$, the trend in H_2 consumption appeared comparable with that of the HT samples, with a poorly resolved maximum evident in the range 450–700 $^\circ\text{C}$.

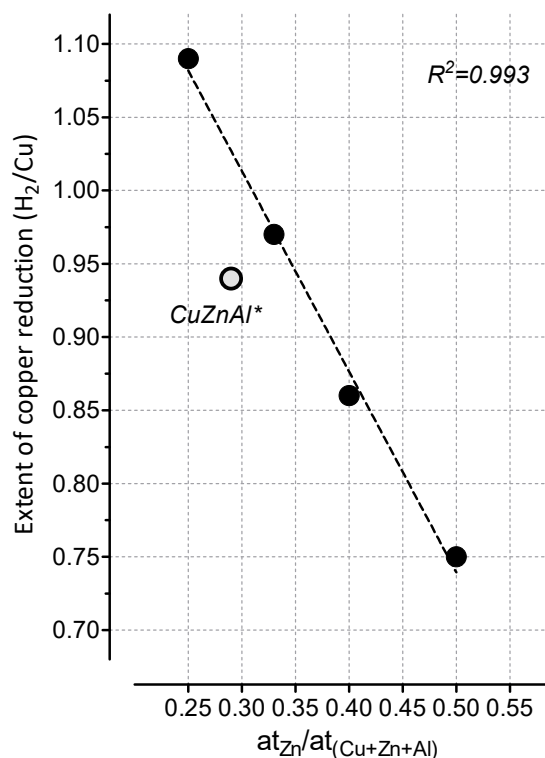


Figure 4. Influence of Zn mole fraction on the extent of copper reduction (H₂/Cu, Table 2).

SEM analysis, reported in Figure 5, showed how the chemical composition of the investigated samples affected the final morphology of the system. In particular, the HT-111 and HT-122 samples exhibited a very porous sponge-like structure composed of predominantly elongated grains (>0.5 μm), whose uniform distribution per unit of surface revealed that some of the CuO species were embedded in the oxide carriers (i.e., ZnO and/or Al₂O₃). Moreover, on HT-112, an evident segregation of large oxide agglomerates of Al₂O₃ (light blue pots) was observable, contrarily to HT-121, where a denser granular structure favored the enrichment of copper species (red pots) among the carrier oxides. Regarding the reference commercial CuZnAl sample, a squamaceous plate-like structure evidenced an important lack of homogeneity in the distribution of the elements, characterized by a general lower porosity, as confirmed by BET analysis. In any case, the EDAX results on the investigated systems showed an elemental concentration in line with the design composition.

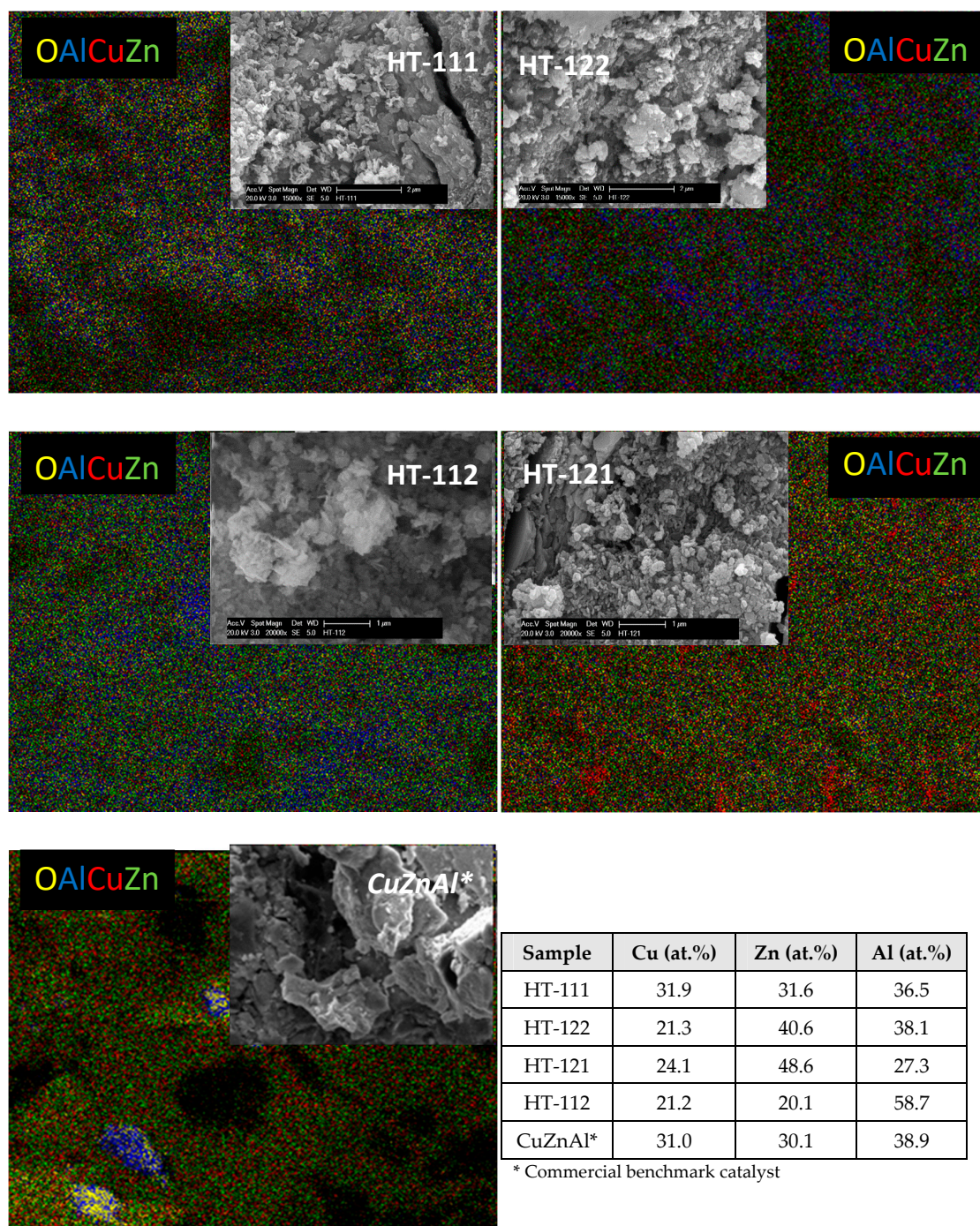


Figure 5. SEM analysis and mapping investigation with results of EDAX analysis.

Considering that copper surface area, dispersion, and crystalline size represent key features critically influencing the adsorption behavior of the reactants and the subsequent conversion of reaction intermediates, in Table 3, the quantitative data of N_2O chemisorption measurements are reported. The reference commercial CuZnAl sample exhibited the largest copper surface area (*MSA*), accounting for a metal dispersion of 17.8%, as the result of particles not being larger than 6 nm. As for the samples prepared using the hydrotalcite method, it can be observed that the catalyst composition affected their surface characteristics. Although the values of *MSA* resulted slightly lower (17.2–24.6 m^2/g) than that on the commercial catalyst (32.4 m^2/g), leading to a minor metal dispersion (11.6%–16.7%), the obtainment of just larger copper particles (6.2–9.0 nm) could result beneficial for catalytic activity,

due not only to a better resistance to the metal sintering during reaction, but also to a more favorable interaction between the metal and the carrier oxide(s) [22,23].

Moreover, considering that CO₂ affinity of the hydrotalcite-like catalysts is strongly dependent on the atomic composition and activation conditions [24], CO₂ desorption measurements were performed on the investigated catalysts, with profiles and quantitative data reported in Figure 6 and Table 3, respectively. It can be recognized that the strength of basic sites was determined by the adsorption and desorption peak of CO₂ in the corresponding temperature range: weak–medium basic sites (below 300 °C) and strong basic sites (above 300 °C).

Table 3. Surface properties of the investigated hydrotalcite-like structures from N₂O single pulse titration and CO₂-TPD measurements.

Catalyst Sample	N ₂ O Titration Pulse			CO ₂ Uptake			N ₂ O/CO ₂
	MSA (m ² /g)	D _{Cu} (%)	d _{Cu} (nm)	mmol/g _{cat}	n ₁ ^(a)	n ₂ ^(b)	
HT-111	24.6	11.7	8.9	0.837	0.28	0.72	0.356
HT-122	20.9	16.7	6.2	0.648	0.10	0.90	0.390
HT-121	17.2	11.6	9.0	0.257	0.16	0.84	0.808
HT-112	22.7	13.6	7.6	0.925	0.18	0.82	0.297
CuZnAl *	32.4	17.8	5.8	0.695	0.29	0.71	0.565

* Commercial benchmark catalyst: (a) population fraction of weak–medium CO₂ sites in the T range <300 °C; (b) population fraction of strong CO₂ sites in the T range >300 °C.

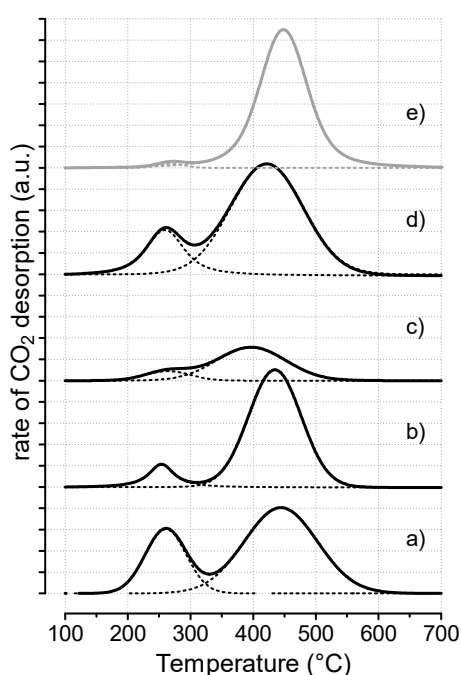


Figure 6. CO₂-TPD profiles of the Cu_xZn_yAl_z catalysts: (a) HT-111; (b) HT-122; (c) HT-121; (d) HT-112; (e) CuZnAl reference sample.

Interestingly, all the catalysts provided similar CO₂-TPD profiles, consisting of a prominent peak (70–90%), with the maximum centered between 380 and 480 °C, attributed to mono- and bidentate carbonates releasing CO₂ from metal–oxygen pairs (Cu⁸⁺) or low-coordination anions (O²⁻), and a smaller peak (displayed below 300 °C) assigned to desorption of bicarbonate species from metallic Cu, very sensitive to the pretreatment phase (reduction temperature and time) and typically considered of scarce catalytic relevance [25–27]. From a quantitative point of view (see data in Table 3), it is evident that a too high content of ZnO depressed the CO₂ adsorption in the HT-121 sample (0.257 mmol_{CO2}/g_{cat}), while, by changing the ratios of M²⁺/M³⁺ metals, significantly higher CO₂

uptakes were recorded. The HT-112 sample exhibited basicity as large as $0.925 \text{ mmol}_{\text{CO}_2}/\text{g}_{\text{cat}}$, evidently due to lower coordination and favorable location of the adsorption sites [28].

2.2. Catalytic Activity

The catalytic behavior of the prepared samples was investigated under CO_2 hydrogenation conditions and, in Table 4, the results obtained at 30 bar in the temperature range of 220–260 °C are reported, in terms of carbon dioxide conversion, methanol selectivity, and methanol yield.

Table 4. Conversion selectivity data ($X_{\text{CO}_2}\text{-}S_{\text{MeOH}}$) and methanol yield (Y_{MeOH}) of hydrotalcite-based and reference catalysts in the CO_2 hydrogenation reaction at different temperatures (P_{R} , 30 bar; GHSV: 8800 $\text{NL}/\text{kg}_{\text{cat}}/\text{h}$).

Catalyst Sample	T_{R} , 220 °C		T_{R} , 240 °C		T_{R} , 260 °C	
	$X_{\text{CO}_2}\text{-}S_{\text{MeOH}}$ (%)	Y_{MeOH} (%)	$X_{\text{CO}_2}\text{-}S_{\text{MeOH}}$ (%)	Y_{MeOH} (%)	$X_{\text{CO}_2}\text{-}S_{\text{MeOH}}$ (%)	Y_{MeOH} (%)
HT-111	9.1–70.7	6.4	13.1–51.7	6.8	18.7–37.6	7.0
HT-122	6.5–62.8	4.1	13.2–41.6	5.5	19.8–30.7	6.1
HT-121	6.2–52.6	3.3	12.6–32.7	4.1	18.5–22.4	4.1
HT-112	6.6–66.6	4.4	12.9–47.3	6.1	19.2–34.6	6.7
CuZnAl *	10.1–57.9	5.9	16.9–43.4	7.3	20.8–34.3	7.1

* Commercial benchmark catalyst.

Under the operating conditions, no methane, hydrocarbons, or coke were found in the reaction products. As it is possible to observe, all the hydrotalcite-derived systems featured a similar catalytic behavior characterized by X_{CO_2} values rising with temperature from 6.2% to 19.8%, counterbalanced by a drop in S_{MeOH} from 70.7% to 22.4%, definitely accounting for methanol yield (Y_{MeOH}) comprised between 4.1% and 7.0%. In particular, the HT-121 sample, at higher Zn/(Cu + Zn + Al) ratio, exhibited considerably low conversion and selectivity levels at each reaction temperature, which corresponded to a maximum $Y_{\text{CH}_3\text{OH}}$ of 4.1% at 260 °C. Under the adopted experimental conditions, the reference CuZnAl catalyst exhibited an activity–selectivity pattern characterized by an increase in CO_2 conversion from 10.1% to 20.8% and a “smoother” decrease in the S_{MeOH} from 57.9% to 34.3%, demonstrating a general performance comparable to that of the HT-111 sample at a similar composition.

Accordingly, productivity methanol data (Figure 7A) displayed analogous STY values of ca. 200 $\text{g}_{\text{MeOH}}/\text{kg}_{\text{cat}}/\text{h}$ for the HT-111 sample and the reference commercial CuZnAl catalyst in the range of temperature considered, while, under the same Cu loading (Figure 7B), an optimum metallic ratio of 0.4 ensured an STY as high as 900 $\text{g}_{\text{MeOH}}/\text{kg}_{\text{Cu}}/\text{h}$ for the HT-122 sample. Indeed, despite having the lowest copper loading, the HT 122 catalyst showed the best catalytic performance, especially at higher temperatures (240–260 °C), wherein the commercial catalyst, unlike the hydrotalcite-like samples, exhibited a reduction of catalytic activity above 240 °C.

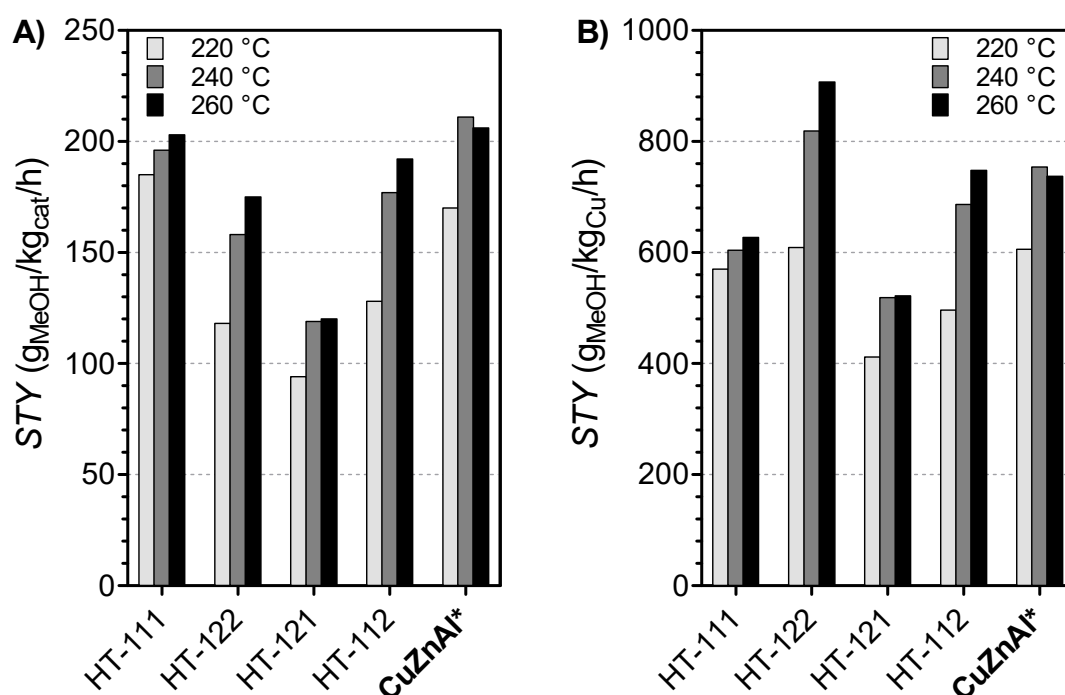


Figure 7. Space–time yield of methanol (STY) calculated per (A) mass of catalyst and (B) Cu loading (PR, 30 bar; GHSV: 8800 NL/kg_{cat}/h).

2.3. Structure–Activity Relationships

In an attempt to rationalize the catalytic behavior, the intrinsic activity of the catalysts was elaborated in terms of turnover frequency of CO₂, calculated as the rate of CO₂ conversion (at 220 °C) on a strong base site.

Although the “real” role and the intrinsic activity of each specific site under CO₂ hydrogenation conditions require more deep investigation and further experiments, Figure 8 shows that the nature of the adsorption sites controlled the CO₂ conversion rate. In particular, the HT-121 sample exhibited the highest turnover frequency of CO₂, revealing an apparent better activity of the system at higher ZnO content compared to all other samples. However, considering the lowest MeOH productivity obtained on the same HT-121 sample (see Figure 7), it is evident that, on such a sample, a higher CO₂ conversion rate was related to a higher activity of the strong CO₂ adsorption site in the parallel reaction of reverse water gas shift, rather than in the direct CO₂ hydrogenation to MeOH, thus favoring the formation of CO at the expense of methanol. In this respect, the surface composition of the sample certainly played a key role, as probed by the EDAX results in Figure 5, which suggests that the highest specific CO₂ activity of the HT-121 sample strongly depended on the specific adsorption capacity induced by the relative ratio among the metal precursors. Indeed, it is generally known that the stabilization of Cu^{δ+} sites, as specific active centers for CO₂ adsorption/activation, can be attributed either to the incorporation of the copper phase into the metal–oxide lattice or to the formation of a definite metal–support interaction, suitable to promote and ensure the progressive hydrogenation rate of CO₂ via several intermediates and transition states until methanol. On the contrary, an evidently weak CO_x adsorption on the catalytic surface sites prevents the sequential hydrogenation via C–O bond dissociation, while enhancing the parallel path of RWGS [29,30]. Since the molar fraction of Zn also affects the metallic properties of the catalyst (see Figure 4), a further elaboration was carried out, considering the rate of methanol formation as a function of the N₂O/CO₂ ratio, taken as a parameter capable of justifying the relative redox contribution of metallic sites with respect to sites of oxide nature (see Figure 9). Indeed, monitoring the concentration of Cu⁰ and Cu⁸⁺ sites, the N₂O/CO₂ ratio actually represented a measure of the extent of the metal/oxide(s) Cu⁰/(CuZnAl)O_x interface.

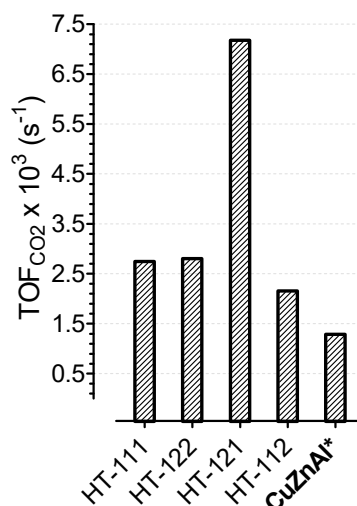


Figure 8. Turnover frequency of CO₂ determined as rate of CO₂ conversion (at 220 °C) on strong CO₂ site.

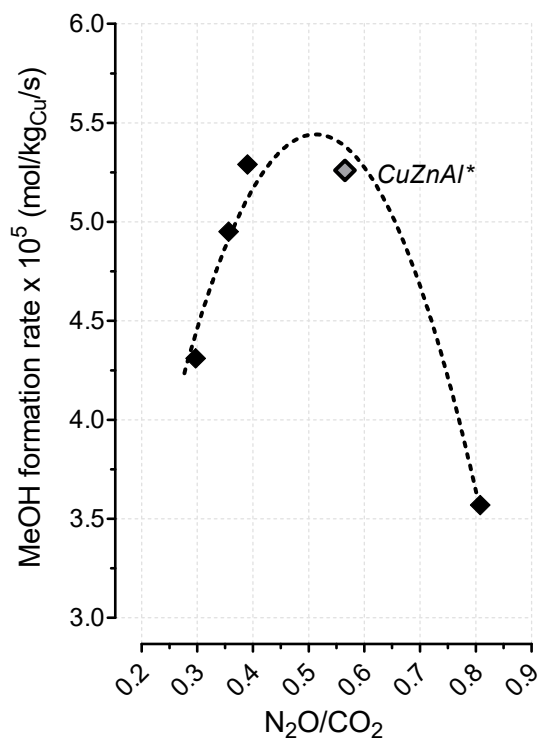


Figure 9. Methanol formation rate (@ 220 °C) vs. CO₂/N₂O ratio.

As it is possible to observe, the specific rate of methanol formation was significantly sensitive both to the number and to the nature of surface sites, since the activation of hydrogen and carbon dioxide on the respective active centers could effectively bring toward the formation of methanol only in the presence of a balanced amount of metallic and oxidized sites. It is so demonstrated that, by tailoring hydrotalcite-derived CuZnAl catalysts with a specific ratio among the metal precursors, it is possible to realize systems characterized by physico-chemical and catalytic features superior to those of commercial catalysts.

3. Materials and Methods

3.1. Catalyst Preparation

$\text{Cu}_x\text{Zn}_y\text{Al}_z$ hydrotalcite-like catalysts with “ $x:y:z$ ” ratios of 1:1:1, 1:1:2, 1:2:1, and 1:2:2 were synthesized by a co-precipitation method at 25 °C. Two aqueous solutions, one containing the metal precursors dissolved in deionized water and another one of NaOH and Na_2CO_3 , were used. $\text{CuSO}_4 \cdot 5\text{H}_2\text{O}$, $\text{Zn}(\text{NO}_3)_2 \cdot 6\text{H}_2\text{O}$, and $\text{Al}(\text{NO}_3)_3 \cdot 9\text{H}_2\text{O}$ (supplied by Carlo Erba, >98% purity, Cornaredo (MI), Italy) were employed as metal precursors. The precipitant solution was added dropwise in 50 mL of mixed metal precursor solution under vigorous stirring. The pH was kept at a constant value of 11. The precipitate obtained was aged at 65 °C for 18 h using a vapor condenser. The resulting paste was filtered and washed with deionized water and subsequently dried for 4 h at 110 °C. The hydrotalcites so obtained were calcined in air at 450 °C for 6 h with a heating rate of 5 °C/min.

3.2. Catalytic Testing

Catalytic testing was carried out in a CO_2 hydrogenation reaction at 30 bar ($\text{CO}_2/\text{H}_2/\text{N}_2 = 23/69/8$). During all the runs, a fixed tubular bed reactor (internal diameter, 4 mm; length, 200 mm), located within a stainless-steel rod to reduce gradients of temperature throughout, was used. The catalytic experiments were carried out at 30 bar, in the temperature range between 220 and 260 °C, by operating at a space velocity of 8800 $\text{NL}/\text{kg}_{\text{cat}}/\text{h}$. A catalyst grain size of 40–70 mesh was selected as a suitable compromise between mechanical resistance of the catalyst particle and pressure drop along the reactor. Before the run, the catalysts were reduced at 300 °C in situ under a “pure” hydrogen flow at atmospheric pressure. A GC equipped with a double-column system, connected to a flame ionized detector (for C-containing products) and thermal conductivity detector (for permanent gases), was used to analyze the reaction stream. The space–time yield of methanol (STY) was determined as the amount in grams of methanol produced per kilogram of catalyst per hour ($\text{g}_{\text{MeOH}}/\text{kg}_{\text{cat}}/\text{h}$).

3.3. Catalyst Characterization

3.3.1. X-Ray Fluorescence Analysis (XRF)

Catalyst composition was analytically determined by an XRF spectrometer (Bruker AXS-S4 Explorer, Milano, Italy), equipped with an Rh X-ray source (Rh anode, 75 μm Be-window). A LiF 220 crystal analyzer and a 0.12° divergence collimator were used to analyze the samples at the solid state, by considering the emission values of copper, zinc, and aluminum transitions (Cu– $\text{K}\alpha_1$, Zn– $\text{K}\alpha_1$, and Al– $\text{K}\alpha_1$).

3.3.2. XRD Characterization

The structure of dried, calcined, and reduced samples was analyzed by a diffractometer (Philips X’Pert, Eindhoven, The Netherlands), operating at 40 kV, 30 mA, and a scan step of 0.05° s^{-1} , with an Ni β -filtered Cu $\text{K}\alpha$ radiation ($\lambda = 1.5406 \text{ \AA}$).

3.3.3. N_2 Physisorption

The textural properties of the catalysts were determined from N_2 adsorption/desorption isotherms at –196 °C, using a Micromeritics ASAP 2020 gas adsorption device (Norcross, GA, USA). The isotherms were elaborated for surface area calculation (S_{BET}), while the Barrett–Joyner–Halenda (BJH) method was used for porosity evaluation.

3.3.4. Temperature-Programmed Reduction (TPR)

Catalyst reducibility was probed under hydrogen atmosphere in a linear quartz micro-reactor (i.d., 4 mm) fed with 5 vol.% H_2/Ar flowing at a rate of 30 STP mL/min. The measurements were carried out in a customized home-made setup plant in the temperature range 20–800 °C at a heating rate of

10 °C/min, with 20–30 mg of sample, properly weighed in order to operate under the same amount of reducible species. Hydrogen consumption was monitored by a thermal conductivity detector, previously calibrated with a known amount of CuO. TPR profiles resulted very reproducible in terms of maximum position (± 3 °C), as well as extent of H₂ consumption ($\pm 3\%$).

3.3.5. N₂O Chemisorption Measurements

“Single-pulse” N₂O titration measurements were performed in the same experimental setup plant of TPR at 90 °C for the determination of copper surface area (*MSA*) and dispersion (*D*_{Cu}). Before measurements the samples were reduced at 300 °C in situ for 1 h under H₂ atmosphere (100 STP mL/min), then “flushed” at 310 °C in nitrogen flow (15 min) and further cooled down at 90 °C. The values of *MSA* and *D*_{Cu} were calculated by assuming a Cu:N₂O = 2:1 titration stoichiometry and a surface atomic density of 1.46×10^{19} Cu_{at}/m², while the average size of copper particle (*d*_{Cu}) was obtained from the conventional formula, d_{Cu} (nm) = 104/*D* (%), by assuming a spherical particle shape.

3.3.6. CO₂ Temperature-Programmed Desorption (CO₂-TPD)

Measurements of temperature-programmed desorption of carbon dioxide (CO₂-TPD) were also performed in the experimental setup used for TPR and N₂O chemisorption to determine the surface concentrations of base sites. Before CO₂-TPD experiments, the catalyst samples (~100 mg) were reduced in a linear quartz micro-reactor (l, 200 mm; i.d., 4 mm), under atmospheric pressure, by flowing hydrogen (100 STP mL/min) from room temperature to 300 °C (heating rate of 10 °C/min). After an isothermal step of 60 min at 300 °C under hydrogen flow, followed by purging with helium, the samples were saturated in a gas mixture of 20 vol.% CO₂/He (flow rate of 50 mL/min) for 60 min. Then, the samples were cooled down to 100 °C in He flow until a constant baseline level was maintained. The desorption measurements were carried out in a range from 100 to 600 °C, at a heating rate of 10 °C/min, using helium as the carrier flow (50 STP mL/min). The evolved gases were monitored by a thermal conductivity detector, previously calibrated by known pulses of CO₂.

3.3.7. Scanning Electron Microscopy (SEM)

SEM analysis was carried out to study the morphology of the ternary CuZnAl catalysts (Philips XL-30-FEG, Eindhoven, The Netherlands). An EDAX analyzer (Oxford, model 6587, Eindhoven, The Netherlands) was used to determine the atomic composition, with specimens of catalyst samples prepared by gold sputtering and deposited as powders on pin flat stubs.

3.3.8. Transmission Electron Microscopy (TEM)

Powdered samples were dispersed in 2-propanol under ultrasound irradiation, and the resulting suspension was added dropwise to a holey carbon-coated support grid. TEM images of the Cu_xZn_yAl_z catalysts were acquired and elaborated by a Philips CM12 instrument (Eindhoven, The Netherlands) equipped with a high-resolution camera.

4. Conclusions

The activity–selectivity pattern of hydrotalcite-derived CuZnAl systems in the hydrogenation of CO₂ to methanol was explored, with evaluation of textural, structural, and surface factors affecting catalytic functionality. The HT method leads to systems characterized by a very homogeneous distribution of metals per unit area, along with a good dispersion of copper. The concentration of Zn controls the surface properties and, in particular, the reducibility of the systems, as well as the stabilization of Cu⁸⁺ sites at the metal/oxide interface, while a balanced “mix” of Cu⁰, Cu⁸⁺, and strong base sites positively affects the rate of methanol formation upon a favorable adsorption/activation of H₂ and CO₂. By tailoring the HT catalysts with a specific ratio among the metal precursors, an activity–selectivity profile superior to that of a commercial reference catalyst is achievable,

demonstrating a methanol productivity as high as 0.9 g/g_{Cu}/h at ca. 10% CO₂ conversion per pass, at 30 bar in the range of temperature considered.

Author Contributions: Conceptualization, L.F. and G.B.; methodology, F.F.; validation, G.B.; investigation, C.C. and S.T.; resources, G.B. and F.F.; data curation, C.C. and S.T.; writing—original draft preparation, L.F.; writing—review and editing, G.B. and F.F.; visualization, C.C.; supervision, F.F.; project administration, F.F.; funding acquisition, G.B.

Funding: The project leading to this submission received funding from the Italian Ministry for Education, University, and Research (MIUR) within the research program PRIN no. 2017WR2LRS.

Conflicts of Interest: The authors declare no conflicts of interest.

References

1. Natesakhawat, S.; Lekse, J.W.; Baltrus, J.P.; Ohodnicki, P.R.; Howard, B.H.; Deng, X.Y.; Matranga, C. Active Sites and Structure–Activity Relationships of Copper-Based Catalysts for Carbon Dioxide Hydrogenation to Methanol. *ACS Catal.* **2012**, *2*, 1667–1676. [[CrossRef](#)]
2. Kunkes, E.L.; Studt, F.; Abild-Pedersen, F.; Schlögl, R.; Behrens, M. Hydrogenation of CO₂ to methanol and CO on Cu/ZnO/Al₂O₃: Is there a common intermediate or not? *J. Catal.* **2015**, *328*, 43–48. [[CrossRef](#)]
3. Behrens, M. Heterogeneous Catalysis of CO₂ Conversion to Methanol on Copper Surfaces. *Angew. Chem. Int. Ed.* **2014**, *53*, 12022–12024. [[CrossRef](#)]
4. Lunkenbein, T.; Schumann, J.; Behrens, M.; Schlögl, R.; Willinger, M.G. Formation of a ZnO overlayer in industrial Cu/ZnO/Al₂O₃ catalysts induced by strong metal–support interactions. *Angew. Chem. Int. Ed.* **2015**, *54*, 4544–4548. [[CrossRef](#)] [[PubMed](#)]
5. Martin, O.; Perez-Ramirez, J. New and revisited insights into the promotion of methanol synthesis catalysts by CO₂. *Catal. Sci. Technol.* **2013**, *3*, 3343–3352. [[CrossRef](#)]
6. Arena, F.; Mezzatesta, G.; Zafarana, G.; Trunfio, G.; Frusteri, F.; Spadaro, L. Effects of oxide carriers on surface functionality and process performance of the Cu–ZnO system in the synthesis of methanol via CO₂ hydrogenation. *J. Catal.* **2013**, *300*, 141–151. [[CrossRef](#)]
7. Schumann, J.; Eichelbaum, M.; Lunkenbein, T.; Thomas, N.; Galvan, M.C.A.; Schlögl, R.; Behrens, M. Promoting strong metal support interaction: Doping ZnO for enhanced activity of Cu/ZnO:M (M = Al, Ga, Mg) catalysts. *ACS Catal.* **2015**, *5*, 3260–3270. [[CrossRef](#)]
8. Baltes, C.; Vukojevic, S.; Schuth, F. Correlations between synthesis, precursor, and catalyst structure and activity of a large set of CuO/ZnO/Al₂O₃ catalysts for methanol synthesis. *J. Catal.* **2008**, *258*, 334–344. [[CrossRef](#)]
9. Muhamad, E.N.; Irmawati, R.; Tautiq-Yap, Y.H.; Abdullah, A.H.; Kniep, B.L.; Girgsdies, F.; Ressler, T. Comparative study of Cu/ZnO catalysts derived from different precursors as a function of aging. *Catal. Today* **2008**, *131*, 118–124. [[CrossRef](#)]
10. Kniep, B.L.; Girgsdies, F.; Ressler, T. Effect of precipitate aging on the microstructural characteristics of Cu/ZnO catalysts for methanol steam reforming. *J. Catal.* **2005**, *236*, 34–44. [[CrossRef](#)]
11. Behrens, M.; Kissner, S.; Girgsdies, F.; Kasatkin, I.; Hermerschmidt, F.; Mette, K.; Ruland, H.; Muhler, M.; Schlögl, R. Knowledge-based development of a nitrate-free synthesis route for Cu/ZnO methanol synthesis catalysts via formate precursors. *Chem. Commun.* **2011**, *47*, 1701–1703. [[CrossRef](#)] [[PubMed](#)]
12. Behrens, M. Meso- and nano-structuring of industrial Cu/ZnO/(Al₂O₃) catalysts. *J. Catal.* **2009**, *267*, 24–29. [[CrossRef](#)]
13. Gao, P.; Li, F.; Zhan, H.J.; Zhao, N.; Xiao, F.K.; Wei, W.; Zhong, L.S.; Wang, H.; Sun, Y.H. Influence of Zr on the performance of Cu/Zn/Al/Zr catalysts via hydrotalcite-like precursors for CO₂ hydrogenation to methanol. *J. Catal.* **2013**, *298*, 51–60. [[CrossRef](#)]
14. Li, C.; Yuan, X.; Fujimoto, K. Development of highly stable catalyst for methanol synthesis from carbon dioxide. *Appl. Catal. A* **2014**, *469*, 306–311. [[CrossRef](#)]
15. Catizzone, E.; Bonura, G.; Migliori, M.; Frusteri, F.; Giordano, G. CO₂ Recycling to Dimethyl Ether: State-of-the-Art and Perspectives. *Molecules* **2018**, *23*, 31. [[CrossRef](#)]

16. Tisseraud, C.; Comminges, C.; Belin, T.; Ahouari, H.; Soualah, A.; Pouilloux, Y.; Le Valant, A. The Cu–ZnO synergy in methanol synthesis from CO₂, Part 2: Origin of the methanol and CO selectivities explained by experimental studies and a sphere contact quantification model in randomly packed binary mixtures on Cu–ZnO coprecipitate catalysts. *J. Catal.* **2015**, *330*, 533–544. [CrossRef]
17. Bonura, G.; Cordaro, M.; Cannilla, C.; Arena, F.; Frusteri, F. The changing nature of the active site of Cu–Zn–Zr catalysts for the CO₂ hydrogenation reaction to methanol. *Appl. Catal. B* **2014**, *152–153*, 152–161. [CrossRef]
18. Kühn, S.; Schumann, J.; Kasatkin, I.; Havecker, M.; Schlögl, R.; Behrens, M. Ternary and quaternary Cr or Ga-containing ex-LDH catalysts—Influence of the additional oxides onto the microstructure and activity of Cu/ZnAl₂O₄ catalysts. *Catal. Today* **2015**, *246*, 92–100. [CrossRef]
19. Kühn, S.; Tarasov, A.; Zander, S.; Kasatkin, I.; Behrens, M. Cu-Based Catalyst Resulting from a Cu, Zn, Al Hydrotalcite-Like Compound: A Microstructural, Thermoanalytical, and In Situ XAS Study. *Chem. Eur. J.* **2014**, *20*, 3782–3792. [CrossRef]
20. Bonura, G.; Khassin, A.A.; Yurieva, T.M.; Cannilla, C.; Frusteri, F.; Frusteri, L. Structure control on kinetics of copper reduction in Zr-containing mixed oxides during catalytic hydrogenation of carbon oxides to methanol. *Catal. Today* **2018**, in press. [CrossRef]
21. Ahouari, H.; Soualah, A.; Le Valant, A.; Pinard, L.; Magnoux, P.; Pouilloux, Y. Methanol synthesis from CO₂ hydrogenation over copper based catalysts. *React. Kinet. Mech. Catal.* **2013**, *110*, 131–145. [CrossRef]
22. Ren, S.; Shoemaker, W.R.; Wang, X.; Shang, Z.; Klinghoffer, N.; Li, S.; Yu, M.; He, X.; White, T.A.; Liang, X. Highly active and selective Cu–ZnO based catalyst for methanol and dimethyl ether synthesis via CO₂ hydrogenation. *Fuel* **2019**, *230*, 1125–1133. [CrossRef]
23. Bao, J.; Yang, G.; Yoneyama, Y.; Tsubaki, N. Significant Advances in C1 Catalysis: Highly Efficient Catalysts and Catalytic Reactions. *ACS Catal.* **2019**, *9*, 3026–3053. [CrossRef]
24. Jung-Il Yang, J.-I.; Kim, J.-N. Hydrotalcites for adsorption of CO₂ at high temperature. *Korean J. Chem. Eng.* **2006**, *23*, 77–80. [CrossRef]
25. Tang, Y.; Liu, Y.; Zhu, P.; Xue, Q.; Chen, L.; Lu, Y. High-Performance HTLcs-Derived CuZnAl Catalysts for Hydrogen Production via Methanol Steam Reforming. *AIChE J.* **2009**, *55*, 1217–1228. [CrossRef]
26. Sikander, U.; Sufian, S.; Salam, M.A. A review of hydrotalcite based catalysts for hydrogen production systems. *Int. J. Hydrog. Energy* **2017**, *42*, 19851–19868. [CrossRef]
27. Debecker, D.P.; Gaigneaux, E.M.; Busca, G. Exploring, Tuning, and Exploiting the Basicity of Hydrotalcites for Applications in Heterogeneous Catalysis. *Chem. Eur. J.* **2009**, *15*, 3920–3935. [CrossRef]
28. Tichit, D.; Coq, B. Catalysis by Hydrotalcites and Related Materials. *Cattech* **2003**, *7*, 206–217. [CrossRef]
29. Daza, Y.A.; Kuhn, J.N. CO₂ conversion by reverse water gas shift catalysis: Comparison of catalysts, mechanisms and their consequences for CO₂ conversion to liquid fuels. *RSC Adv.* **2016**, *6*, 49675–49691. [CrossRef]
30. Pastor-Pérez, L.; Shah, M.; le Saché, E.; Ramirez Reina, T. Improving Fe/Al₂O₃ Catalysts for the Reverse Water-Gas Shift Reaction: On the Effect of Cs as Activity/Selectivity Promoter. *Catalysts* **2018**, *8*, 608. [CrossRef]

